

AN INTER-COMPARISON EXERCISE ON THE CAPABILITIES OF CFD MODELS TO PREDICT THE SHORT AND LONG TERM DISTRIBUTION AND MIXING OF HYDROGEN IN A GARAGE

A.G. Venetsanos¹, E. Papanikolaou¹, M. Delichatsios^{1,10}, J. Garcia², O.R. Hansen³, M. Heitsch⁴, A. Huser⁵, W. Jahn⁶, T. Jordan⁷, J-M. Lacombe⁸, H.S. Ledin⁹, D. Makarov¹⁰, P. Middha³, E. Studer¹¹, A.V. Tchouvelev¹², A. Teodorczyk¹³, F. Verbecke¹⁰, M.M. van der Voort¹⁴

¹ Environmental Research Laboratory, National Centre for Scientific Research Demokritos (NCSR), Aghia Paraskevi, Attiki, 15310, Greece, venets@ipta.demokritos.gr

² Escuela Técnica Superior de Ingenieros Industriales, Universidad Politécnica de Madrid (UPM), José Gutiérrez Abascal, 2, E-28006 Madrid, Spain

³ GEXCON AS, (GXC) Fantoftvegen 38 Box 6015 Postterminalen N-5892 BERGEN Norway

⁴ Gesellschaft für Anlagen-und Reaktorsicherheit (GRS)mbH, Research Management Division Schwertnergasse 1, 50667 Köln

⁵ Det Norske Veritas (DNV) AS Energy Solutions, Oslo, Norway

⁶ Forschungszentrum Juelich, (FZJ) 52425 Juelich, Germany

⁷ IKET, Forschungszentrum Karlsruhe, (FZK) Postfach 3640, 76021 Karlsruhe, Germany

⁸ Explosion-Dispersion Unit, Institut National de l'Environnement industriel et des RISques (INERIS), Parc Technologique Alata, BP2, F-60550 Verneuil-en-Halatte, France

⁹ Health and Safety Laboratory, (HSL) Harpur Hill, Buxton, Derbyshire, SK17 9JN, UK

¹⁰ FireSERT Institute, University of Ulster, (UU) Newtownabbey, BT37 0QB, Northern Ireland, UK

¹¹ Heat Transfer and Fluid Mechanics Laboratory, Commissariat à l'Energie Atomique, (CEA) F-91191 Gif-sur-Yvette Cedex, France

¹² A.V.Tchouvelev & Associates Inc. (AVT) 6591 Spinnaker Circle, Mississauga, ON L5W 1R2, CA

¹³ Warsaw University of Technology, (WUT) Poland

¹⁴ TNO Defence, Security and Safety Process Safety and Dangerous Goods P.O. Box 45 2280 AA Rijswijk, The Netherlands

Abstract

The paper presents the results of the CFD inter-comparison exercise SBEP-V3, performed within the activity InsHyde, internal project of the HYSAFE network of excellence, in the framework of evaluating the capability of various CFD tools and modeling approaches in predicting the physical phenomena associated to the short and long term mixing and distribution of hydrogen releases in confined spaces. The experiment simulated was INERIS-TEST-6C, performed within the InsHyde project by INERIS, consisting of a 1 g/s vertical hydrogen release for 240 s from an orifice of 20 mm diameter into a rectangular room (garage) of dimensions 3.78x7.2x2.88 m in width, length and height respectively. Two small openings at the front and bottom side of the room assured constant pressure conditions. During the test hydrogen concentration time histories were measured at 12 positions in the room, for a period up to 5160 s after the end of release, covering both the release and the subsequent diffusion phases. The benchmark was organized in two phases. The first phase consisted of blind simulations performed prior to the execution of the tests. The second phase consisted of post-calculations performed after the tests were concluded and the experimental results made available. The participation in the benchmark was high: 12 different organizations (2 non-HYSAFE partners) 10 different CFD codes and 8 different turbulence models. Large variation in predicted results was found in the first phase of the benchmark, between the various modeling approaches. This was attributed mainly to differences in turbulence models and numerical accuracy options (time/space resolution and discretization schemes). During the second phase of the benchmark the variation between predicted results was reduced.

1 INTRODUCTION

Understanding of the conditions under which small to medium hydrogen releases (up to 1g s⁻¹) in confined spaces become dangerous is a key objective of the InsHyde internal project of the HYSAFE Network of Excellence program funded by EC. Within this framework a blind benchmark exercise

was organized in order to further evaluate the various CFD codes and modeling approaches available in HYSAFE, in predicting hydrogen distribution in a garage both during the release phase (short term) and during the diffusion phase, i.e. after stop of the release period (long term). In parallel an experimental investigation of the hydrogen distribution field within the garage was organized and performed by INERIS.

Previous HYSAFE experience on CFD benchmarking for hydrogen releases in a hermetically sealed cylinder was presented in [1]. Previous experimental/theoretical work on hydrogen or helium releases in confined spaces has been reviewed by [2]. Further experimental work regarding H₂ releases from BMW cars equipped with LH₂ storage has been reported in [3].

2 EXPERIMENTAL DESCRIPTION

The INERIS “garage” is roughly rectangular in shape with average dimensions 7.2 x 3.78 x 2.88 m in length, width and height respectively, see Figure 1, resulting in effective volume of 78.38 m³. The height of the facility is not constant. The garage ceiling is flat while the distance to ground ranges from 2.85 to 2.92 m, see [4] for a more detailed description. It is located in rock, so that three of the four walls, the roof and ceiling, will remain at the same temperature throughout the duration of the experiment. The fourth sidewall (the front side) is made up of a curtain or plastic sheeting, which will be hermetically sealed. The walls have a surface roughness of five to 10 mm. Two small vents, each with 0.05 m diameter, are located on the wall with plastic sheeting. The centers of the two vents are located 0.075 m above the floor and a distance of 0.075 m on either side of the centre plane.

Gaseous hydrogen is de-pressurized external to the garage, then transported in 3 mm diameter pipe into the stabilization chamber located within the garage. The chamber is 0.265 m in height and has an internal diameter of 0.12 m. The chamber contains a 30-40 mm thick layer of dispersion bed particles, with diameters in the range 10 to 15 mm, in order to homogenize the flow. The dispersion bed is located halfway up the chamber and the hydrogen pipe releases the gas into the chamber at a point below the dispersion bed. The gas is released into the garage through a circular orifice of 20 mm diameter located on the top surface of the chamber. The hydrogen flow rate is 1 g s⁻¹ and the release duration 240 s.

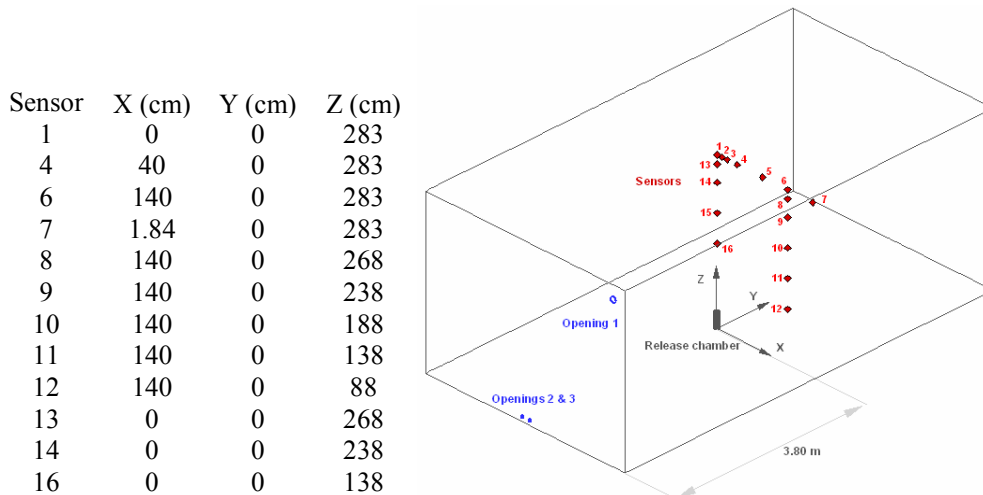


Figure 1 Experimental facility with openings at the front side, the source and the concentration sensors.

3 BENCHMARK DESCRIPTION

Table 1 shows that the participation in the blind and post benchmark exercise was large: 12 organizations, two of which were non-HYSAFE partners (AVT and GRS), with 10 different CFD codes applying 8 different turbulence models. Code name for each case is defined using a combination

of a key for the turbulence model and a key for the organization. During the blind phase experimental results were not available. In the post calculations experimental data were available to all participating organizations. Table 2 shows the main modifications in modeling strategy between post and blind calculations. Table 3 shows the space and time resolution options used in the various cases for the blind calculations.

Table 1 Participation in the calculations (^A: Submission time after deadline)

Case	Turbulence model	CFD Code	Blind calculations run time (s)	Post calculations run time (s)
	Analytical [5]	-	240	
LEVEL_AVT	LEVEL	PHOENICS 3.6 [6]	5400 ^A	0-240 s LEVEL, 240-5400 s laminar
LEVEL_NCSR		ADREA-HF [7]	5400	5400
ML_CEA	Mixing length	CAST3M	5400	800
KE_DNV_a	Standard k-ε [8] with buoyancy effects	FLACS 8.1	800	
KE_DNV_b		KFX	240	240
KE_FZJ		CFX 10.0 [9]	5400 ^A	5400
KE_FZK		GASFLOW 2.4.12	5400	5400
KE_GRS		CFX 10.0	337 ^A	
KE_GXC		FLACS 8.1	5400	
KE_NCSR		ADREA-HF	5400	5400
KE_TNO		FLUENT 6.2	-	240
KE_UPM		FLUENT 6.2 [10]	5400	0-240 k-ε, 240-2980 laminar
REAL_WUT		Realizable k-ε	FLUENT	785
RNG_AVT	RNG k-ε	PHOENICS 3.6	5400 ^A	0-240 s RNG k-ε, 240-5400 s laminar
SST_GRS	SST	CFX 10.0	0-438 s, 438-1043 ^A	905
SST_HSL		CFX 5.7.1	5400	5400 s, CFX 10.0
LES_NCSR	LES Smagorinsky	FDS 4.0	110	2000
VLES_UU	LES- RNG	FLUENT 6.2.16	5400	5000 s, LES Smagorinski-Lilly

Table 2 Main modifications with respect to blind calculations

Case	Modifications
LEVEL_AVT, RNG_AVT	Time step 0.05 s for 60-240 s , Laminar for period 240-5400 s
LEVEL_NCSR, KE_NCSR	GXC release grid, SMART convective scheme, time step 0.02 s for 3-240 s
ML_CEA	GXC release grid, 0.05-0.2 s for release and 0.2 s for diffusion, 1 cm mixing length
KE_DNV_b	Improved grid resolution two times in the z direction and turbulent Schmidt number change from 0.9 to 0.7
KE_FZJ	215346 tetrahedral elements
KE_FZK	GXC release grid, Turbulent Sc = 0.7
KE_TNO	80000 cells block structured, 30 points along orifice diameter, 2 nd order upwind scheme with Van Leer limiter, 1s from 1-240 s
KE_UPM	Half garage (167960 cells), 0.01 for 0-10, 0.1 s for 10-413, 1 s for 413-5400 s, Laminar during diffusion period
SST_GRS	114150 cells, hydrogen diffusivity reduced from 109 to 10 x 10 ⁻⁵ m ² /s
SST_HSL	671690 cells for 0-300 s, 134514 cells for 300-5400 s
LES_NCSR	400000 cells, Smagorinski constant Cs = 0.12, 0.001 s for release and 0.014 for diffusion
VLES_UU	GXC release grid, LES Smagorinski-Lilly model with Cs = 0.1, time step 0.05 s for release, 0.1 s for diffusion

Table 3 Space and time resolution options (blind calculations)

Case	Domain / Grid / Convective scheme	Time step , Time scheme
LVEL_AVT and RNG_AVT	Half garage, 38×52×35 cells, 8 cells of 0.0044 m each for half the orifice, Hybrid scheme	0.005 s for 0-1 s; 0.01 s for 2-5 s; 0.025 s for 6-10 s; 0.05 s for 11-60 s; 0.1 s for 61-240 s; 0.8 s for 241-400 s; 2 s for 401-1000 s; 4 s for 1001-5400 s, First order fully implicit
LVEL_NCSR and KE_NCSR	Half garage, extended 1m beyond door, 27x91x37 cells, 1cm horizontal, 2cm vertical, FOU (first order upwind) scheme	0.01-0.05 s for 3-240 s and 1 s for 260-5400 s, Fully implicit 2 nd order
ML_CEA	2 nodes in the orifice radius, 2 nd order in space	0.05 s from 240-360 s and then a gradual increase up to 1 s, Semi-implicit first order
KE_DNV_a	Full garage, 37506 Structured, One grid cell in the jet outlet	
KE_DNV_b	Full garage, 97104 cells Structured, One grid cell in the jet outlet, Upwind scheme, (90 % 2 nd order, 10 % 1 st order)	0.1 s for 240-1180 s, Implicit
KE_FZJ	Half garage, 69654 cells (tetrahedral), H2 source is a semi circle composed of 14 cell faces and side lengths between ~ 3 and ~ 10 mm., High resolution scheme	0.0001-0.05 s for 0-1 s, 0.05 s for 1-240 s, 0.05-0.5 s for 240-560 s, 0.5 s for 560-1290, 1 s for the rest, Second order
KE_FZK	Full garage, 31 x 59 x 45 cells, 1.861 cm x 1.772 cm x 3.5 cm, FOU scheme	0.0005 s for release, 0.001-0.02 s for diffusion, First order explicit
KE_GRS and SST_GRS	Full garage, 147500 structured, 7500 unstructured cells, High Resolution (2 nd order), 48 cells in the orifice 112 cells across chamber	0.08-2 s, 2 nd order
KE_GXC	Full garage, 0.9m beyond door, 29 x 46 x 33 cells during 0-500 s, One grid cell in the jet outlet, 5 cm from the floor to the top of the release chamber with smooth transition to 10 cm further from the orifice, 9 x 18 x 29 cells during 500-5400 s, Kappa schemes with weighting between 2 nd order upwind and 2 nd order central difference. Delimiters are used for some equations	0.00567 s for 240-5400 s, first order
KE_UPM	335920 structured hexahedral mesh, 1.7 mm close to source, Second order upwind	0.01 for 0-10, 0.1 s for 10-240, 1 s for 240-1000 s, 10 s for 240-5400 s, First order implicit
REAL_WUT	Grid size near inlet mean value =70 mm	0.0001 s for 240-5400 s, 2 nd order implicit
SST_HSL	205821 (six layers of prismatic cells in the near-wall region and tetrahedral cells elsewhere), mesh size is between 0.0024 m and 0.003 m in the region near the orifice, FOU for k, ε, ω (frequency) For other variables 20% FOU and 80% CDS (central differences)	0.5 s for 240-5400 s, 2 nd order
LES_NCSR	550000 cells structured	0.001 s for release
VLES_UU	160928 (unstructured tetrahedral), 0.015 m in vicinity of the hydrogen inflow, ~ about 0.03 m close to vents, ~ 0.15-0.20 m in the rest of the domain, Power law scheme	0.0025 s for release, up to 1 s for diffusion, implicit

4 RESULTS AND DISCUSSION

In order to perform a qualitative and quantitative evaluation of the overall SBEP (Standard Benchmark Exercise Problem) results mean hydrogen concentrations were calculated by averaging the individual time series for each sensor and each CFD case or experiment. Release and diffusion phases have been treated separately. An averaging period from 30 to 240 s was used for the release phase and from 300 to 5400 s for the diffusion phase.

Calculated mean experimental molar concentrations C_o (%) are presented in Table 4. Ratios between predicted (C_p) and observed mean hydrogen concentrations, as function of sensor number with different symbols for each CFD case are shown in Figure 2 and Figure 3 for the blind and post calculations of the release phase and in Figure 6 and Figure 7 for the blind and post calculations of the diffusion phase respectively. For the cases where post calculations were not performed, blind phase results were used in the post-phase figures.

Quantitative evaluation of the SBEP results was performed using statistical performance measures. Mean relative bias (MRB) and mean relative square error (MRSE) were used in this work, to quantify bias and spread, because they are considered more balanced with respect to high and low concentration values than other measures, see [11]. Table 4 presents the calculated MRB and MRSE values for each sensor. In the definition of MRB and MRSE given below over-bars denote averaging over all CFD cases for a given sensor. Optimum values of MRB and MRSE are zero, denoting zero bias and spread respectively. A positive MRB shows that the model overestimates the experimental data.

$$MRB \equiv 2 \overline{\left(\frac{C_p - C_o}{C_p + C_o} \right)}, \quad MRSE \equiv 4 \overline{\left(\frac{C_p - C_o}{C_p + C_o} \right)^2}$$

Table 4 Mean experimental concentrations (molar %), Mean Relative Bias (MRB) and Mean Relative Square Error (MRSE) over all CFD runs for each sensor

Sensor	Release phase					Diffusion phase				
	C_o (%)	Blind		Post		C_o (%)	Blind		Post	
		MRB	MRSE	MRB	MRSE		MRB	MRSE	MRB	MRSE
1	7.34	0.12	0.08	0.11	0.05	7.37	-0.33	0.14	-0.15	0.04
4	5.97	0.00	0.01	0.03	0.01	7.36	-0.33	0.14	-0.15	0.04
6	5.30	-0.06	0.02	0.00	0.02	7.39	-0.33	0.14	-0.15	0.04
7	4.69	0.05	0.02	0.11	0.03	7.21	-0.30	0.13	-0.13	0.03
8	4.70	-0.06	0.03	-0.01	0.02	7.19	-0.31	0.13	-0.13	0.03
9	3.78	0.00	0.02	0.08	0.02	6.84	-0.29	0.12	-0.11	0.03
10	3.07	-0.12	0.06	-0.06	0.02	5.57	-0.19	0.06	-0.04	0.01
11	0.66	0.55	0.73	0.44	0.38	2.87	0.24	0.07	0.18	0.07
12	0.06	0.93	2.04	0.36	1.69	0.89	0.76	0.79	0.17	0.62
13	6.52	0.27	0.14	0.25	0.10	7.29	-0.32	0.14	-0.14	0.04
14	8.04	0.16	0.12	0.15	0.07	6.84	-0.29	0.12	-0.11	0.03
16	16.50	0.06	0.16	0.13	0.09	2.75	0.28	0.10	0.20	0.10

4.1 Release phase

Before comparing the CFD predictions with the present experimental data, it is important to compare the data with other experiments or available correlations. It is well known [12] that the jet flow can be divided into three regions according to the relative importance of buoyancy: the non-buoyant jet region (NBj for $z/L_{Mo} \leq 0.5$), the buoyant jet region (BJ for $0.5 \leq z/L_{Mo} \leq 5$) and the buoyant

plume region (BP for $z/L_{Mo} \leq 5$), where z here denotes the vertical distance from the source and L_{Mo} is the Morton length scale (≈ 0.23 m in the present experiment). In the definitions below ω is the ratio between ambient (air) and density at source (hydrogen), which is approximately 14.4 and F is the densimetric Froude number (≈ 513).

$$L_{Mo} = F^{1/2} \omega^{-1/4} d \quad , \quad \omega = \frac{\rho_a}{\rho_0} \quad , \quad F = \frac{\rho_0 U_0^2}{(\rho_a - \rho_0) g d}$$

Table 5 presents hydrogen molar concentrations for sensors 13-16 calculated using the correlation for axi-symmetric buoyant plumes suggested by [13]. For sensor 16, which lies marginally inside the buoyant jet region use was also made of the correlation reported in [14] valid for this region. The applied correlations are given below in terms of mass fraction (f) similarity. Also shown in Table 5 are molar concentrations calculated under the Boussinesqu approximation ($f \ll 1$). The relationship between molar concentration and mass fraction given below under this approximation becomes: $C_{Bous} \approx \omega f$.

$$f_{BP} = 9.35 \left(\frac{z}{d} \right)^{-\frac{5}{3}} (\omega F)^{\frac{1}{3}} \frac{1}{\omega} \quad , \quad f_{BJ} = 4.4 \left(\frac{z}{d} \right)^{-\frac{5}{4}} F^{\frac{1}{8}} \omega^{\frac{7}{16}} \frac{1}{\omega} \quad , \quad C = \frac{\omega f}{1 + f(\omega - 1)}$$

Table 5 Concentration and jet region for sensors 13-16 from similarity compared with experiment

Sensor	z/L_{Mo}	Region	C_{Bous} (vol. %)	C (vol. %)	Co (%)
16	4.79	BJ	20.11 (22.21 for BP)	16.94 (18.40 for BP)	16.50
15	6.94	BP	12.00	10.80	-
14	9.09	BP	7.67	7.16	8.04
13	10.39	BP	6.15	5.82	6.52

Table 5 shows that the present mean axial experimental concentration in the plume region are higher compared to the Chen and Rodi (1980) correlations. Larger mean concentrations and narrower plumes were also reported in the measurements by Dai et al. [15]. These authors suggested a coefficient value of 10.73 instead of the value of 9.35 suggested by Chen and Rodi and the much lower value of 7.75 suggested by George et al. [16]. For sensor 16 on the other hand the experimental concentration is lower compared to the buoyant jet correlation of Paranjpe (2004) as well as that of Ogino et al. [17], who reported a coefficient value of 4.8 instead of 4.4 for Paranjpe.

The CFD predictions are examined next. A general observation for the blind calculations is that predicted mean concentrations were generally in the range of factor of 2 (from 1/2 to 2 times) with respect to experiment. Such spread was expected given the blind character of the exercise as well as previous experience [1]. Figure 2 and Table 4 show that the maximum spread is observed for sensors 11 and 12, located far from the jet axis and closest to ground. From the remaining sensors those lying along the jet axis (1, 13, 14, 16) present the highest spread, with a maximum observed for sensor 16. The high spread for sensor 16 was unexpected, since this sensor is located the closest to the source. For the post calculations of the release phase Figure 3 shows that the spread has been reduced but not significantly. Table 4 shows that MRSE values were improved by 44% for sensor 16, 17% for sensor 12 and 48 % for sensor 11.

The observed variation between various predictions can in general be attributed to differences in the physical models applied, to differences in the numerical options or to differences in both. Below the various predictions are examined in groups of same turbulence model. This way one can trace any spread between predictions to numerical options. Discussion will be focused on sensor 16 for which

predicted concentration time series compared to experiment are presented in Figure 4 for the blind and Figure 5 for the post calculations.

In the blind phase good agreement between predicted and observed hydrogen concentration for sensor 16 was obtained by GXC and DNV_a employing the standard k- ϵ model and the same code. Good agreement was also obtained by KE_FZK but employing a turbulent Schmidt number of 0.3 in contrast to 0.7 used by GXC and DNV_a. All other blind standard k- ϵ model results overestimated the concentration on sensor 16, with one exception KE_FZJ who underestimated. The highest overestimation was obtained in the case of DNV_b. The successful prediction of GXC and DNV_a can be attributed mainly to the grid, the time step and the convective scheme used. The convective scheme used was of second order accuracy but was not specified in detail.

NCSR D post phase results for sensor 16 showed good agreement with the DNV_a blind results, in contrast to the blind phase predictions. NCSR D used a turbulent Schmidt number of 0.7 in both blind and post calculations. Post calculations were performed using the GXC grid, the SMART convective scheme (up to 3rd order accuracy) and a maximum convective CFL number of 2. Separate sensitivity post calculations showed that the increase of the accuracy of the convective scheme and the decrease in time step both result to reduce the concentration, while the effect of using the GXC grid was to increase the concentration. Calculations performed on the same GXC grid with max CFL = 10 gave mean hydrogen concentration 24.2% for the FOU scheme and 20.1% for SMART. Calculations performed on the same grid with the SMART scheme showed that a decrease in max CFL from 10 to 2 (decrease in time step from 0.02 to 0.004 s) resulted in a decrease of mean concentration from 20.1 to 18.4 %. An increase in the accuracy of the convective scheme was expected to lead to less horizontal spreading and consequently higher hydrogen concentrations, due to hydrogen mass conservation. Calculations showed the opposite and this can be attributed to the fact that the more accurate convective scheme resolves higher velocity gradients, which give rise to higher mechanical turbulent energy production which in turn results in higher mixing and eventually lower concentrations. The effect of the convective scheme was also verified by sensitive calculations performed by TNO.

The importance of the turbulent Schmidt number during the release phase was already noted above. FZK standard k- ϵ model results showed good agreement in the blind phase and overestimation in the post phase. This behavior is attributed to a change in the turbulent Schmidt number from 0.3 in the blind to 0.7 in the post phase. FZK and NCSR D used the same grid in their post calculations. The difference in the predicted concentration is attributed to the more accurate convective scheme used by NCSR D. A turbulent Schmidt number change from 0.9 to 0.7, along with increased vertical grid refinement were the two reasons identified by DNV_b as being responsible for the improvement of their post phase predictions. In the case of FZJ the underestimation of concentrations during the blind phase was removed using a fined grid. In the case of UPM post phase results showed same level of overestimation as in the blind phase but with significant oscillations, which were attributed to the symmetry assumption, which was not used in the blind phase. It should be noted that similar oscillations were not reported in other CFD cases employing the same model and same symmetry assumption.

For the standard k- ϵ model in general, the present results in Figure 3 show that the model tends to overestimate the concentrations on the sensors located along the jet axis. While it is well established, see [18], that for axi-symmetric non buoyant jets this model underestimates the axial concentrations, its behavior for axi-symmetric buoyant jets and plumes is not a clearly solved issue, due to the large variations observed between experimental data existing in the literature. In another work [19] Sanderson showed that the standard k- ϵ model overestimates concentrations compared to Chen and Rodi experiments, while underestimates concentrations compared to the more data of Dai et al. [15].

Regarding other models, RNG k- ϵ model and Realizable k- ϵ model applied by AVT and WUT respectively showed tendency to overestimate the concentrations in the jet region. LVEL calculations performed by AVT and NCSR D, show that this model has the tendency to underestimate the measured

concentrations. Generalized mixing length model calculations performed by CEA underestimated concentration on sensor 16 in the blind phase, but showed significant improvement in the post phase, possibly due to the new grid. LES Smagorinski calculations performed by NCSR D show that the default Smagorinski constant $C_s = 0.2$ used in the blind phase results in significant overestimation of concentrations, while a value of 0.12 gives concentration in close agreement to the experiment. SST model calculations performed by HSL and GRS show that this model has the tendency to produce hydrogen concentrations in the jet region lower than the standard k- ϵ model and in better agreement with the present experiment.

Finally the effect of modeling the release at the interior of the release chamber was taken into account in the cases KE_GXC, KE_GRS, SST_HSL and SST_GRS. In the remaining cases the release was assumed from the top of the chamber with a flat velocity profile. Sensitivity tests by GRS with SST model showed that the first approach, which is more realistic, leads to slightly higher hydrogen concentrations along the jet axis.

4.2 Diffusion phase

Before comparing the computational results to the experimental it is important to consider experimental and computational hydrogen mass balance during the diffusion phase. The experimental total hydrogen mass variation with time was approximately calculated by INERIS using the measured hydrogen concentrations time series and assuming seven horizontally homogeneous layers between the ceiling the sensors and the floor, with heights 5, 15, 30, 50, 50, 50 and 88 cm respectively. It was shown that there was a limited uncontrolled linear mass loss of the order of 0.01 g/s, with the total hydrogen mass dropping from 263 g at 322 s to 210 g at 5400 s. On the other hand, in the blind and post diffusion phase calculations the total hydrogen mass was practically constant, approximately equal to 240 g in most cases, corresponding to 1g/s for 240 s. The deviation of the experimental total hydrogen mass from the preset value of 240 g was considered acceptable for further comparison with the present CFD results.

The predicted mean concentrations are shown in Figure 6 for the blind phase. It can be observed that mean concentrations are in the range of factor of 2 with respect to experiment. It can be observed that the models generally tend to under predict the concentrations at the sensors located closer to the ceiling and over predict the concentrations at the sensors closest to the ground (sensors 11, 16 and 12). This behavior suggests the explanation that the models generally tend to over predict turbulent mixing during the diffusion phase. The highest spread in predicted mean concentrations is observed for sensors 11, 16 and 12, with a maximum for sensor 12, being the closest to the ground. The predicted mean concentrations for the post phase are shown in Figure 7. The two abovementioned figures along with Table 4, summarizing the statistical results, show that both bias (MRB) and spread (MRSE) have been reduced in the post phase. Detailed comparison between predicted and experimental concentration time series for sensor 12 are shown in Figure 8 and Figure 9 for the blind and post phase respectively.

Reasons identified as being mainly responsible for the improvement of the predictions in the post phase were the time step restriction, the reduction of vertical grid spacing and the increase in the order of the convective scheme. The molecular diffusivity of hydrogen in air used in the various CFD cases was between 6.1 and 7.7 ($\times 10^{-5}$ m²/s), with the exception of GEXCON who used a value of 20.0 (default in FLACS) and GRS with a value of 109.0 (due to a typing error). In the post phase the SST_GRS results were improved (less mixing) and GRS attributed this to the molecular diffusivity reduced by one order of magnitude. Laminar flow was forced during the post diffusion phase, by explicitly turning the turbulence model off, in three of the cases: LVEL_AVT, RNG_AVT and KE_UPM. Results for flammable volume (see below) were improved compared to the corresponding blind calculations for two of these cases: RNG_AVT and KE_UPM. Given that in the other CFD cases excessive diffusion was avoided without the option of “manually” turning the turbulence model off suggests that this option cannot be regarded as a general rule.

For risk assessment it is important to know the flammable mixture volume and flammable hydrogen mass distribution in space and time. The predicted flammable mixture volume as function of time for each CFD case is shown in Figure 10 and Figure 11 for the blind and post phases respectively. Blind predictions show two types of physical behavior, either approximately constant stratification or fast transition to homogeneous hydrogen distribution in the room. It is noted that the second behavior is associated with the total flammable mixture volume becoming zero, since the corresponding mean hydrogen concentration would be 3.53% (2.76 m³ released hydrogen homogeneously distributed in a 78.38 m³ room). The corresponding experimental behavior can be drawn from Table 4. Mean experimental concentrations reported in Table 4 for the diffusion phase show that a layer of hydrogen exists close to the ceiling, which is horizontally quasi homogeneous and vertically stratified with the limit of the flammable cloud between sensors 10 and 11. This gives an estimated experimental flammable volume between 27.2 and 40.8 m³. Therefore it can be concluded that predicted flammable volumes below and above these limits should rather be considered as not corresponding to experimental behavior.

5 CONCLUSIONS

A blind and post CFD benchmark exercise was organized within HYSAFE in order to evaluate various modeling approaches in predicting the physical phenomena associated to the short and long term mixing and distribution of hydrogen releases in confined spaces. The experiment simulated was INERIS-TEST-6C. The performed analysis led to the following conclusions:

The effect of the turbulence model is clearly important. In the jet region during the release phase the standard k- ϵ model when applied without previous knowledge of the experimental data (blind prediction) generally tended to overestimate the concentrations. This was shown to be rectified either using a low turbulent Schmidt number (0.3) in combination with a first order upwind scheme or using the usual value of 0.7 for turbulent Schmidt combined with a smaller time step and higher order convective scheme. From the two approaches the second is recommended. RNG k- ϵ and Realizable k- ϵ models showed tendency to overestimate the concentrations. LVEL model generally tended to underestimate concentrations. The SST model was found to produce hydrogen concentrations in the jet region lower than the standard k- ϵ model and in better agreement with the present experiment. The LES Smagorinski model was found in good agreement with measured concentrations when the Smagorinski constant was set equal to 0.12.

In the diffusion phase blind predictions showed two types of physical behavior, either approximately constant stratification or fast transition to homogeneous hydrogen (non-flammable) distribution in the room. Experiments showed that a layer of hydrogen exists close to the ceiling, which is horizontally quasi homogeneous and vertically stratified. Improvement of the predictions and reduction of spread between models was achieved in the post phase mainly by applying time step restrictions, reduction of vertical grid spacing and increase of the order of the convective scheme. The option of “manually” turning the turbulence model off although improved predictions in some cases cannot be suggested as a general recommendation. Comparison between predicted and observed concentrations shows that the models generally tend to overestimate turbulent mixing.

Finally the whole exercise helped the HYSAFE consortium as well as the external collaborating organizations in obtaining consensus regarding issues associated with prediction of hydrogen releases in confined spaces. Further CFD benchmark exercises are planned within HYSAFE in the near future.

6 ACKNOWLEDGEMENTS

The authors would like to thank the European Commission for funding of this work in the framework of the HYSAFE FP6 Network of Excellence (contract no. SES6-CT-2004-502630). TNO contribution was in cooperation between TNO and the University of Technology Delft (Dr. M.J.B.M. Pourquie).

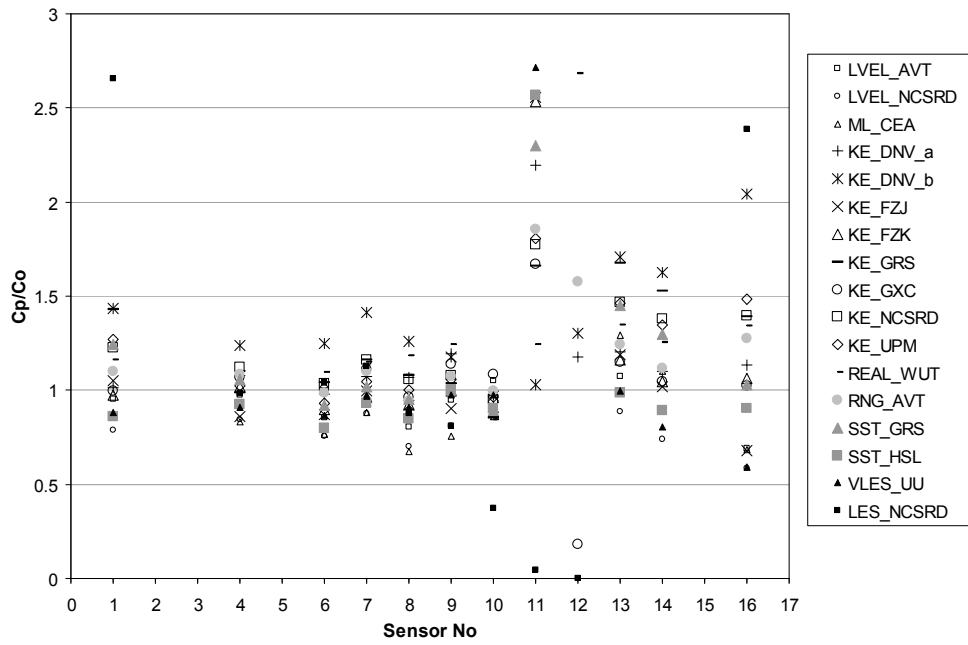


Figure 2 Ratio between predicted and observed mean hydrogen molar concentration during blind release phase

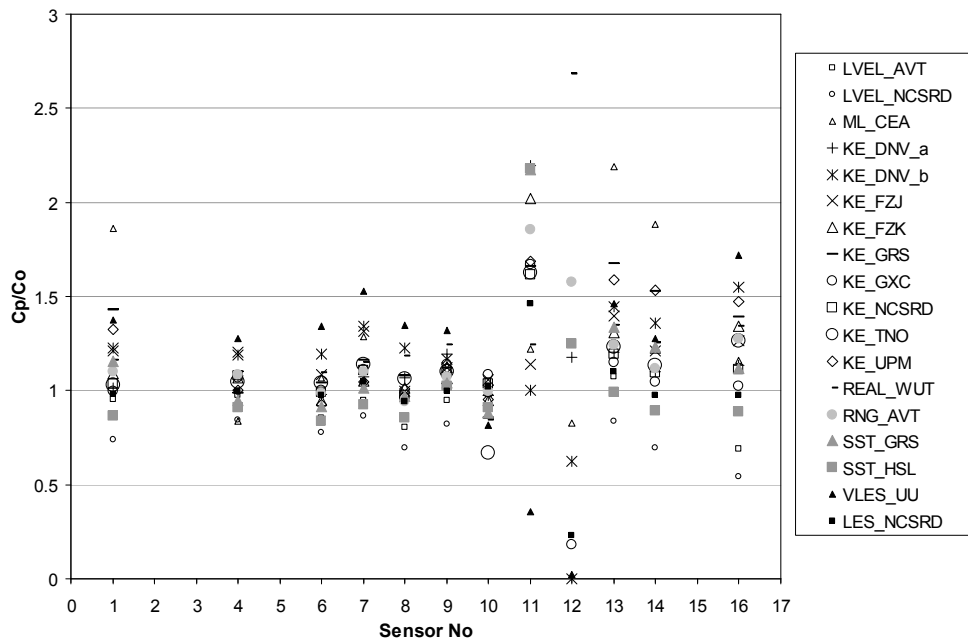


Figure 3 Ratio between predicted and observed mean hydrogen molar concentration during post release phase

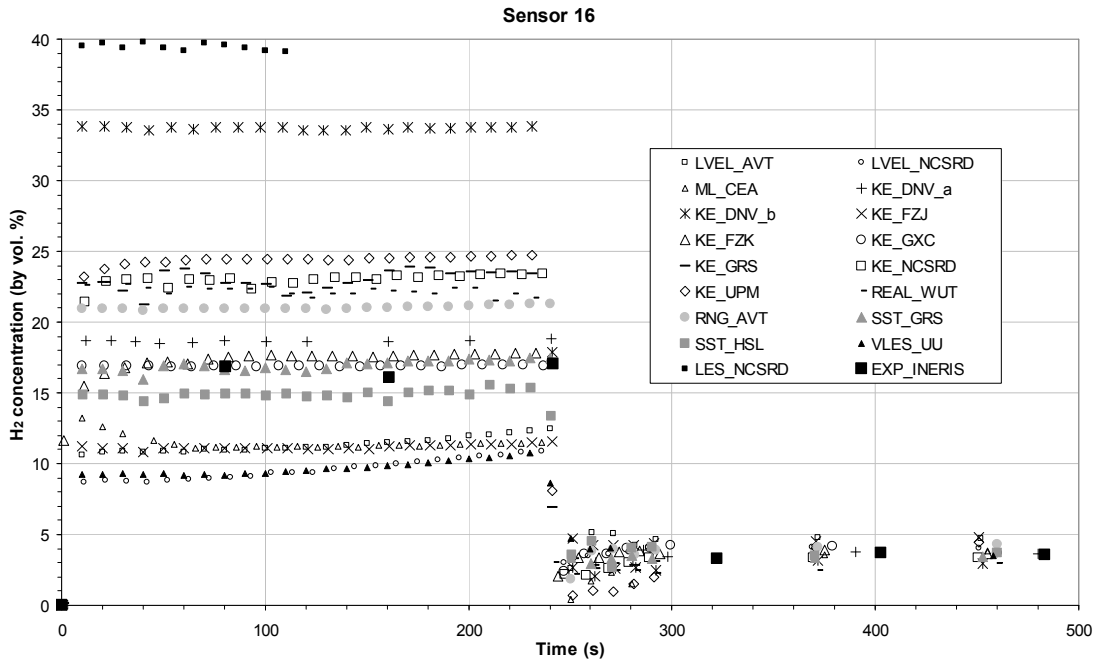


Figure 4 Predicted hydrogen concentration (vol. %) histories for sensor 16 (blind calculations)

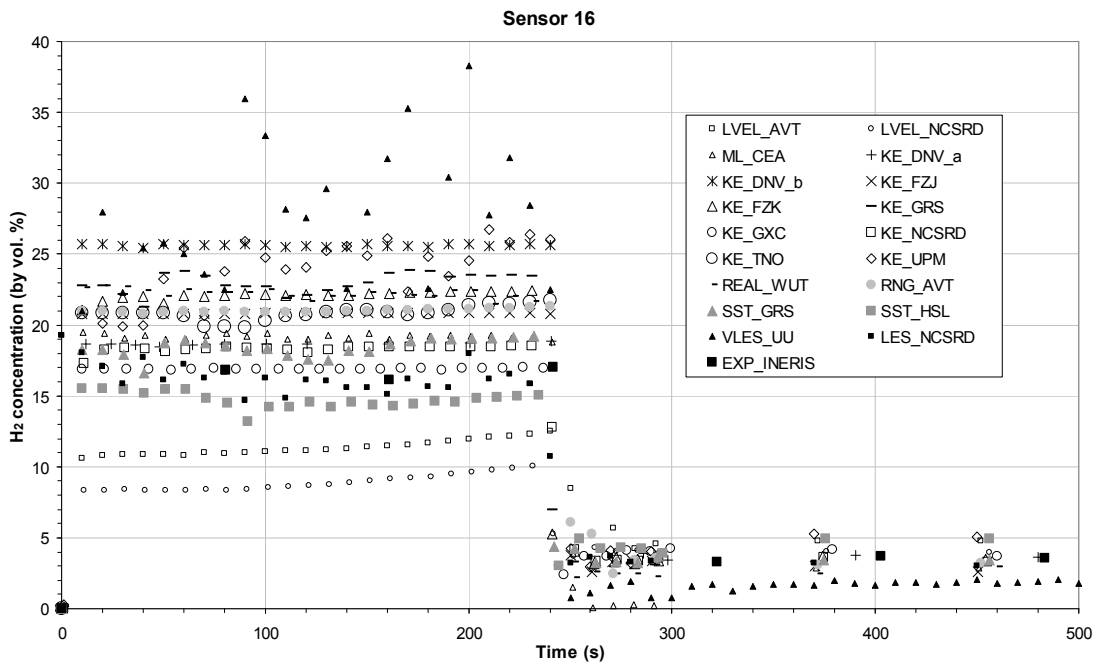


Figure 5 Predicted hydrogen concentration (vol. %) histories for sensor 16 (post calculations)

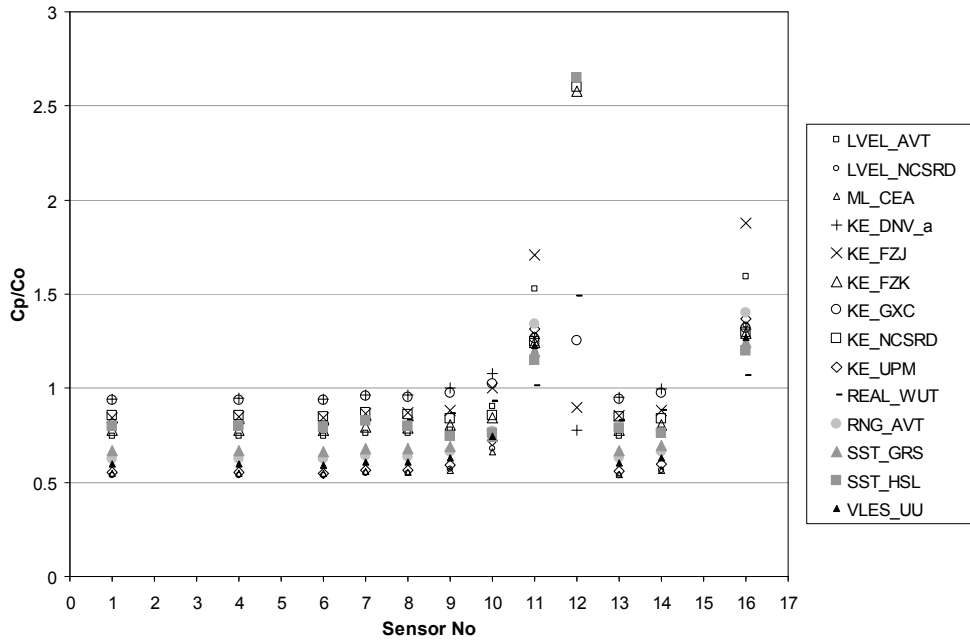


Figure 6 Ratio between predicted and observed mean hydrogen molar concentration during blind diffusion phase

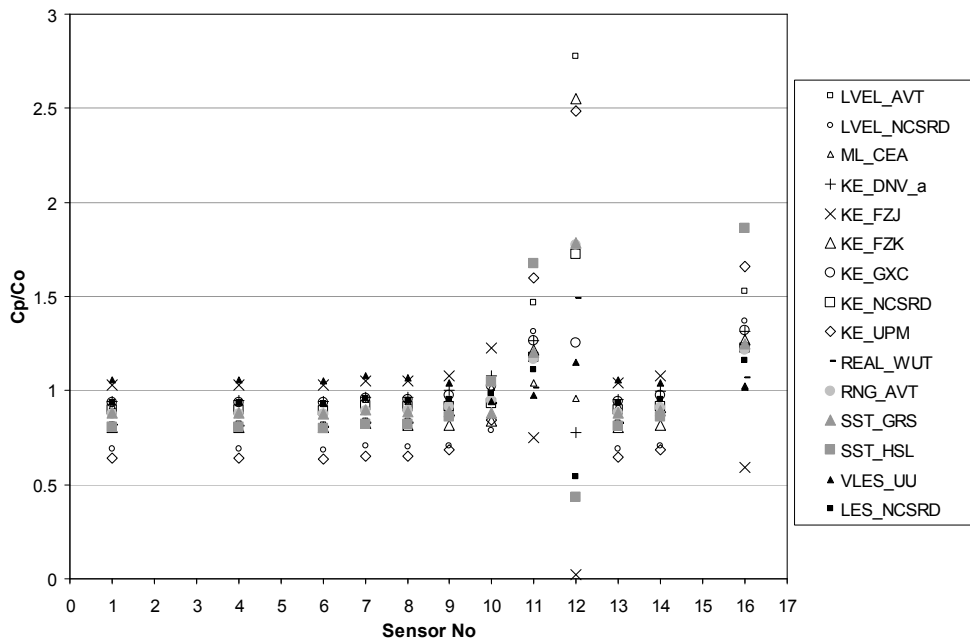


Figure 7 Ratio between predicted and observed mean hydrogen molar concentration during post diffusion phase

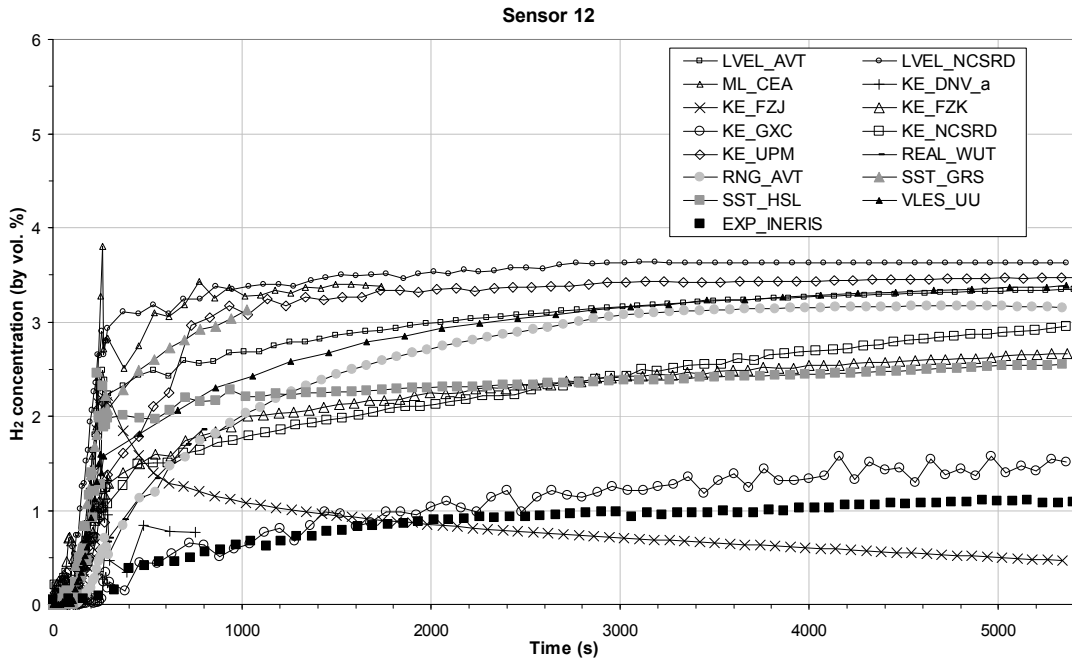


Figure 8 Predicted hydrogen concentration (vol. %) histories for sensor 12 (blind calculations)

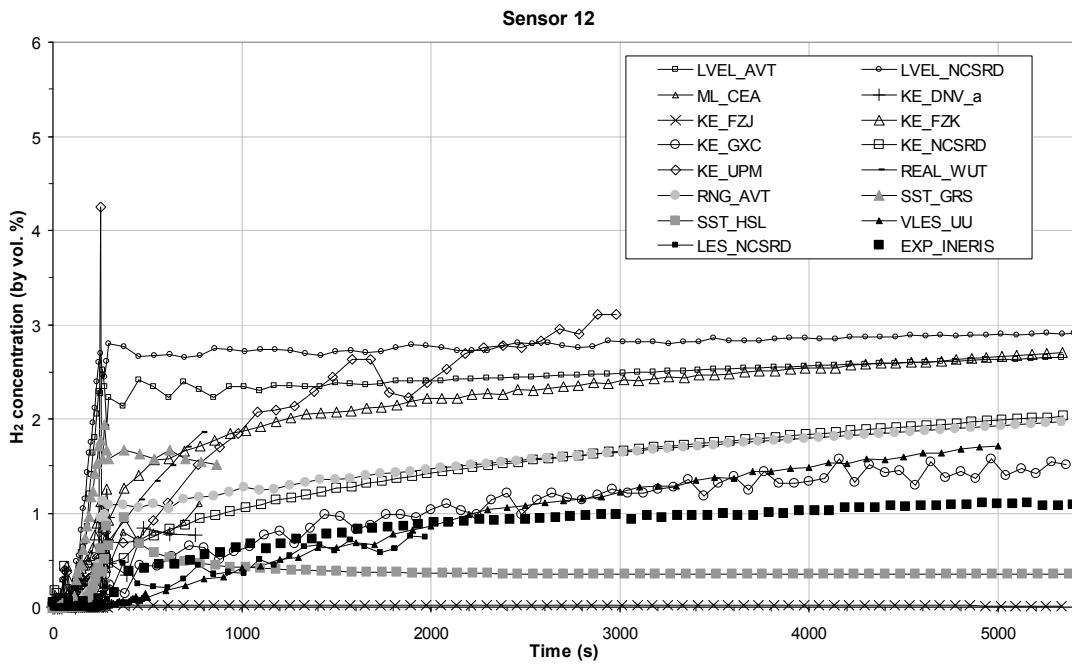


Figure 9 Predicted hydrogen concentration (vol. %) histories for sensor 12 (post calculations)

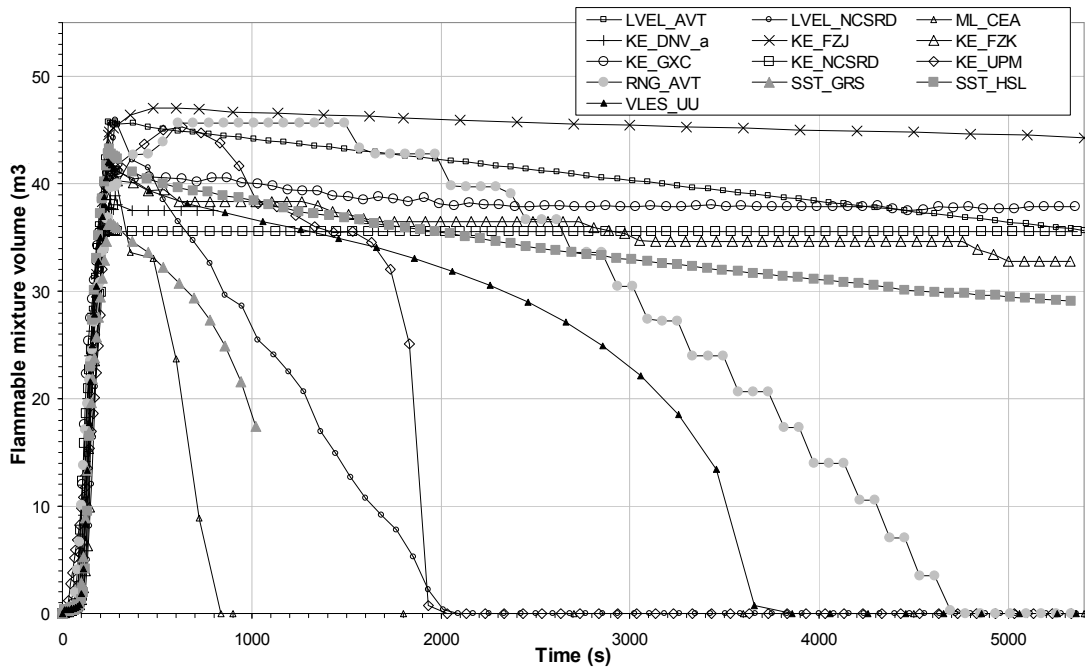


Figure 10 Predicted flammable mixture volume histories (blind calculations)

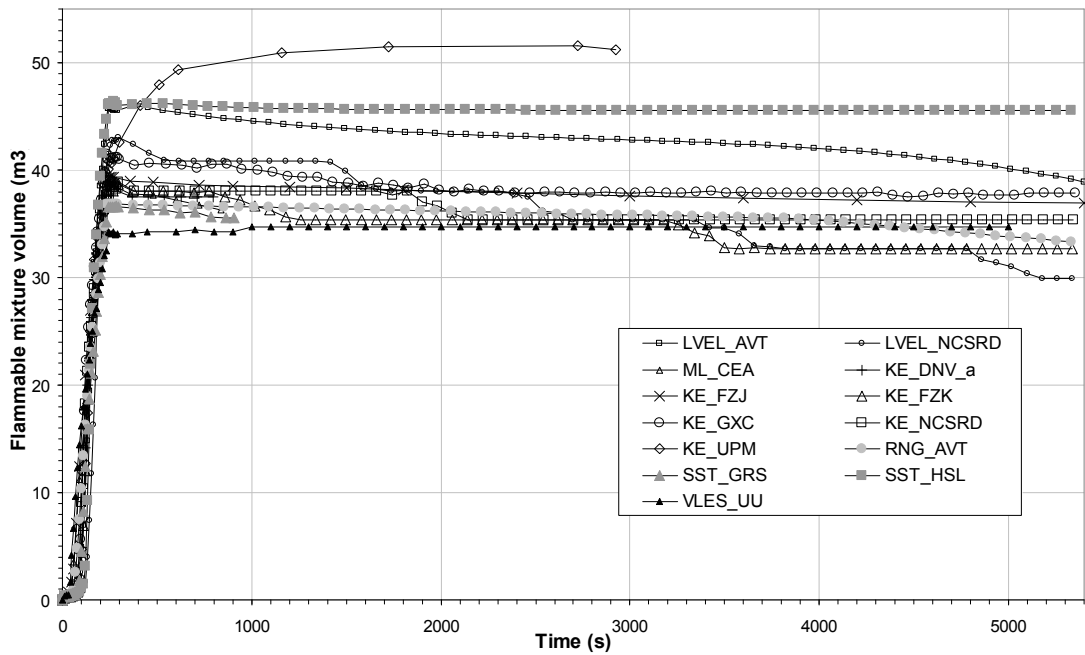


Figure 11 Predicted flammable mixture volume histories (post calculations)

7 REFERENCES

- [1] Gallego E., Migoya E., Martin-Valdepenas J.M., Crespo A., Garcia J., Venetsanos A.G., Papanikolaou E., Kumar S., Studer E., Dagba Y., Jordan T., Jahn W., Oiset S., Makarov D., An Inter-comparison Exercise on the Capabilities of CFD models to predict distribution and mixing of H₂ in a closed vessel, In print Int. J. Hydrogen Energy, 2007

-
- [2] Papanikolaou E.A., Venetsanos A.G., CFD Modelling for Slow Hydrogen Releases in a Private Garage without Forced Ventilation, International Conference on Hydrogen Safety, Pisa, Italy, 8-10 September, 2005
- [3] Fürst, S., Dub, M., Gruber, M., Lechner, W. and Müller, C, "Safety of hydrogen-fueled motor vehicles with IC engines", ICHS Conference Pisa 2005
- [4] Dagba Y., Perette L., Venetsanos A.G., Description of INERIS-test-6 experiment and requirements for corresponding blind SBEP in the framework of the InsHyde internal project, HYSAFE report, 24 October 2005
- [5] Delichatsios M.A., Closed form approximate solutions for smoke filling in enclosures including the volume expansion term, Fire Safety Journal 38, 2003, pp. 97-101.
- [6] http://www.cham.co.uk/phoenics/d_polis/d_docs/tr000.htm
- [7] Bartzis J.G., ADREA-HF: A three dimensional finite volume code for vapour cloud dispersion in complex terrain, EUR report 13580 EN, 1991.
- [8] Launder B.E. and Spalding D.B., "The numerical computation of turbulent flow", Computer Methods in Applied Mechanics and Engineering, 3, Issue 2, pp. 269-289, 1974
- [9] <http://www.ansys.com/products/cfx.asp>
- [10] <http://fluent.com/software/fluent/>
- [11] Duijm N.J., Ott S., Nielsen M., An evaluation of validation procedures and test parameters for dense gas dispersion models, Journal of Loss Prevention in the Process Industry, Vol 9, No 5, 1996, pp. 323-338.
- [12] Panchapakesan N.R. and Lumley J.L., Turbulence measurement in axisymmetric jets of air and helium, part 2. Helium Jet, J. Fluid Mech., Vol. 246, 1993, pp. 225-247.
- [13] Chen C.J. and Rodi W., Vertical Turbulent Buoyant Jets - A review of Experimental Data, HMT-4. Pergamon, 1980
- [14] Paranjpe S., Remote Detection of Hydrogen Leaks Using Laser Induced Rayleigh/Mie Scattering, MSc Thesis, University of Florida, 2004
- [15] Dai Z., Tseng L-K., Faeth G.M., Structure of Round, Fully Developed, Buoyant Turbulent Plumes, J. Heat Transfer, Vol. 116, 1994, pp. 409-417
- [16] George W.K., Alpert R. L. and Tamanini F., Turbulence measurements in an axi-symmetric buoyant plume, Int. J. Heat Mass Transfer 20, 1977, pp. 1145-1154
- [17] Ogino F., Takeuchi H., Kudo I., Mizushina T., Heated Jet Discharged Vertically into Ambients of Uniform and Linear Temperature Profiles, Int. J. Heat Mass Transfer 23, 1980, pp. 1581-1588
- [18] Wilcox D.C. Turbulence modelling for CFD, 1994, DCW Industries Inc., 456 p.
- [19] Sanderson V.E. Turbulence modelling of turbulent buoyant jets and compartment fires, PhD Thesis, Cranfield University 2001, 248 p.